Article

Salicylideneanilines-based Covalent Organic Frameworks as Chemo-Selective Molecular Sieves

Guo-Hong Ning, Zixuan Chen, Qiang Gao, Wei Tang, Zhongxin Chen, Cuibo Liu, Bingbing Tian, Xing Li, and Kian Ping Loh

J. Am. Chem. Soc., **Just Accepted Manuscript** • Publication Date (Web): 15 Jun 2017

Salicylideneanilines-based Covalent Organic Frameworks as Chemo-Selective Molecular Sieves

Guo-Hong Ning,[1] Zixuan Chen,[1] Qiang Gao,[1] Wei Tang,[2] Zhongxin Chen,[1] Cuibo Liu,[1] Bingbing Tian,[1] Xing Li[1] and Kian Ping Loh[1*]

[1]*Department of Chemistry, National University of Singapore, 3 Science Drive 3, Singapore 117543*

[2]*Institute of Materials Research and Engineering, A*STAR, 2 Fusionopolis Way, Innovis, Singapore 138634, Singapore.*

ABSTRACT: Porous materials such as covalent-organic frameworks (COFs) are good candidates for molecular sieves due to the chemical diversity of its building blocks, which allows fine-tuning of its chemical and physical properties by design. Tailored synthesis of inherently functional building blocks can generate framework materials with chemo-responsivity, leading to controllable functionalities such as switchable sorption and separation. Herein, we demonstrate chemo-selective, salicylideneanilines-based COF (SA-COF), which undergo solvent-triggered tautomeric switching. This is unique compared to solid-state salicylideneanilines counterpart, which typically requires high energy input such as photo or thermal activation to trigger the enol-keto tautomerisim and *cis-trans* isomerization. Accompanying the tautomerization, the ionic properties of the COF can be tuned reversibly, thus forming the basis of size-exclusion, selective ionic binding or chemo-separation in SA-COF demonstrated in this work.

Introduction

Covalent organic frameworks (COFs) are a class of crystalline porous polymer that allows atomically precise integration of functionalities into an extended, porous network.[1-5] Although COFs have great application potentials in wide ranging fields including gas storage,[6,7] energy storage,[8-10] drug delivery,[11] catalysis[12-14] and electronic application,[15-17] molecular separation on the basis of size, charge and functionality by using COFs' ordered pores and channels are not widely reported. One challenge is the difficulty in tailoring the interactions between pore surface and sorbents. Wang's group used pre-synthetic modification to prepare the thioether-functionalized COF-LZU8 for sensing and removal of mercury (II) ions.[18] Jiang's group improved CO_2 adsorption by postsynthetic modification of COFs' pore surface with various functional groups.[7] Incorporating inborn functionalities into the pores which can interact with molecules based on non-covalent interactions are attractive due to the ability to engender a chemo-responsive response to the environment. One strategy is to construct the COF from monomers which can undergo dynamic structural changes *via* coordination or non-covalent interactions, *i.e.* protonation-induced tautomerization or *cis-trans* isomerization. Triggered by environmental cues (solvent and pH), dramatic changes in the acidic character or ionicity of the functional groups occurs following tautomrization and *cis-trans* isomerization, thus imparting inborn selectivity to targeted molecules in the pores. In actuality, the properties of the porous framework structure are often different from the building blocks due to the cross-linking and tight packing of the molecular layers. The rigidity of the COF framework can also restrict the rotational or flexural motions of the building blocks. Thus far there are no reports of reticular synthesis of COF, which can undergo solvent-triggered tautomerization.

Scheme 1. Reversible proton tautomerism of salicylideneanilines under themo- and photo-chromism pathway. The *trans*-keto form bears two accessible hydrogen-bonding sites.

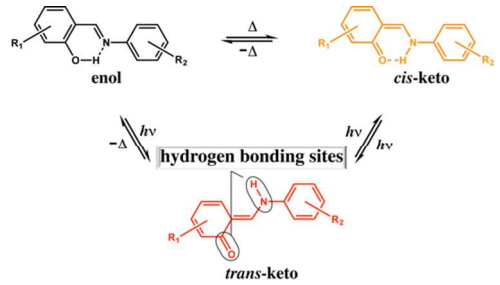

Salicylideneanilines (**SA**), a class of Schiff base comprising salicylaldehyde and aniline derivatives, have attracted great attentions due to their unique photo- and thermo-chromic properties in the solid-state, which can find applications in sensors, optical data storage and displays devices.[19-22] The mechanism of reversible color change of **SA** in response to external simulation (*i.e.* temperature and light) in the solid-state is well studied and suggests a tautomeric structural transformation promoted by proton transfer.[23-25] Firstly, an equilibrium exists between the white colored enol form at lower temperature and the yellow colored *cis*-keto form at room temperature (r.t.), and in both forms, a cyclic intermediate stabilized by intramolecular hydrogen bonding is observed (Scheme 1.). Secondly, the isomerization between the *cis*-keto and the red colored *trans*-keto form can be induced by light.[23,24] The resulting *trans*-keto form relaxes back to the *cis*-keto form *via* thermo- or photo-isomerization (Scheme 1).[25] Accompanying the reversible color change of **SA**, the hydrogen and ionic

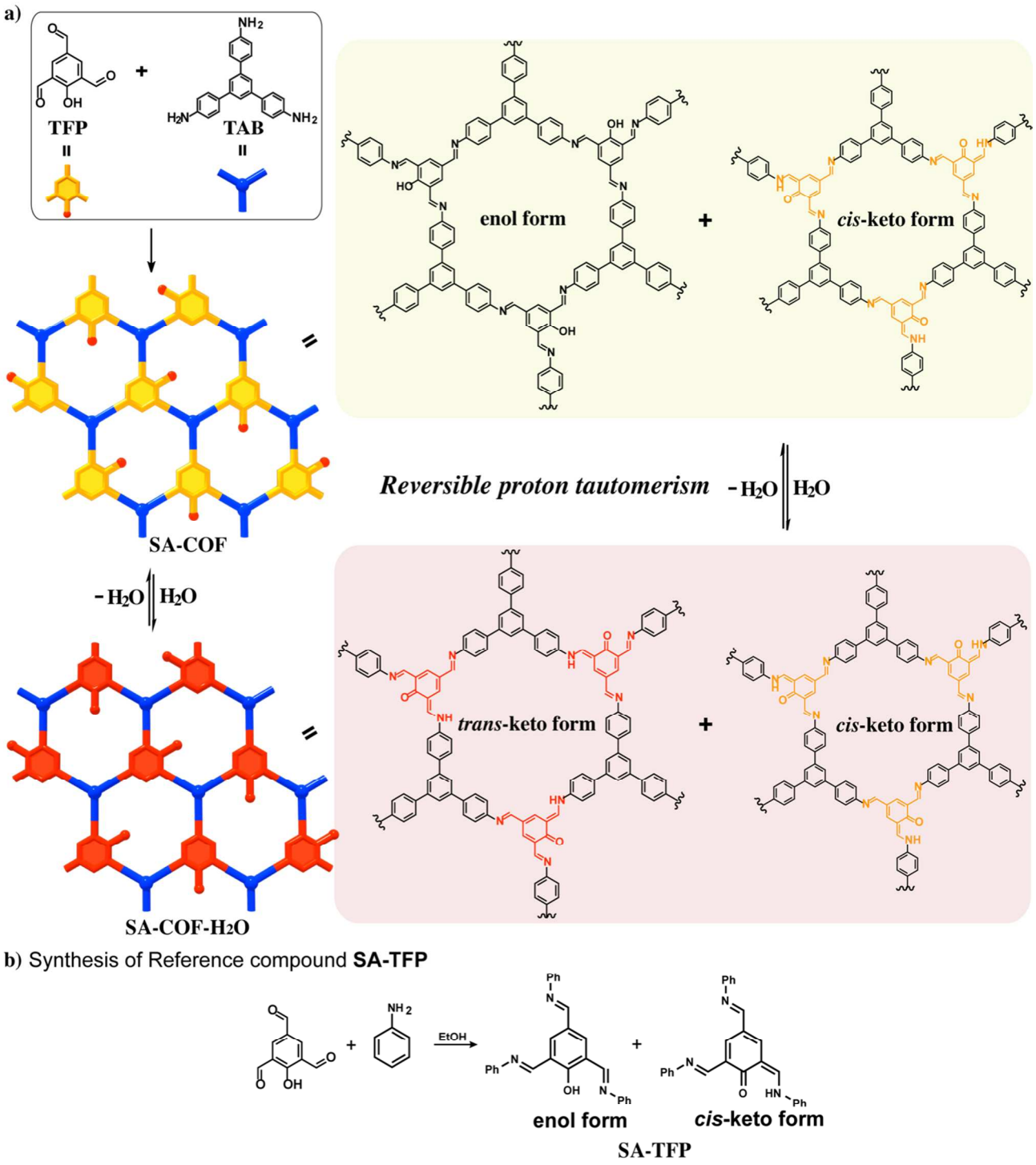

Figure 1. a) Conceptual representation for synthesis of solvatochromic **SA-COF** and reversible proton tautomerism triggered by water adsorption and desorption; b) synthesis of reference compound **SA-TFP**.

bonding properties of **SA** changes dramatically during the proton tautomerism (slight acidic in enol form and basic in *cis*- and *trans*-keto form) (Scheme 1).

The reversible switching of functionality in **SA** motivated us to consider integrating **SA** moieties into COFs to make **SA-COF**. Interestingly, **SA-COF** exhibits reversible proton tautomerism triggered by adsorption and desorption of water molecules (Fig. 1). This is the first report that the transformation between *cis*- and *trans*-keto form in solid-state can be initiated by low energy input *i.e.* solvent, instead of high energy input *i.e.* photo-irradiation. Importantly, the tautomerization allows a dynamic change in the ionic properties of the pores in response to chemical cues, thus forming the basis of size-exclusion or selective ionic binding. The tunable functionality of pore surface allows **SA-COF** to bind to positively charged molecules in basic condition, while

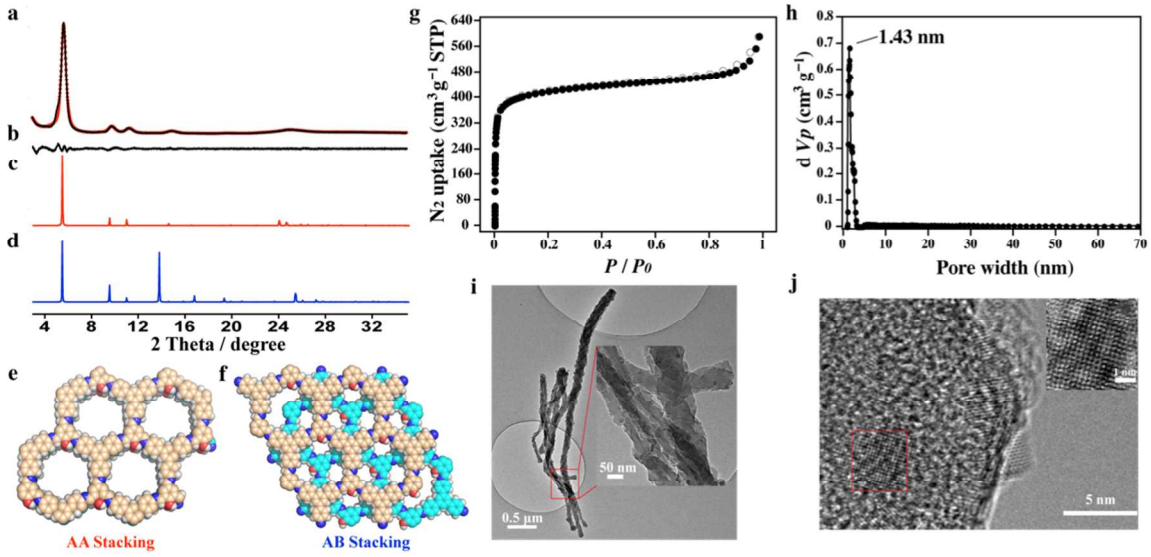

Figure 2. Crystal structure analysis, isotherm profiles of N_2-gas sorption and electronic microscope image of **SA-COF**. **a**, Experimental (black line) and refined (red dots) PXRD pattern of **SA-COF**. **b**, Difference curve between experimental and refined PXRD patterns. **c** and **d**, Simulated PXRD pattern of **SA-COF** with AA (red line) and AB (blue line) stacking structure. **e** and **f**, Top view of the optimized **SA-COF** in the eclipsed AA stacking and staggered AB stacking mode shown as space filing model. **g**, N_2 adsorption (filled) and desorption (open) isotherm profiles of **SA-COF** (STP, standard temperature and pressure). **h**, Pore-size distribution of **SA-COF** calculated by non-local DFT modeling based on N_2 adsorption data. **i** and **j** showing high resolution TEM image of **SA-COF** and arrangement of the micro-spores in crystalline domain.

excluding it in acidic condition. More interestingly, **SA-COF** selectively binds molecules with aromatic hydroxyl groups over aromatic amino groups following conversion to the *trans*-keto stage (Scheme 1).

Experimental Section

Synthesis of SA-COF. TFP (14.3 mg, 0.80 mmol), **TAB** (27.5 mg, 0.80 mmol), 0.5 mL of *n*-butanol, 0.5 mL of 1,2-dichorobenzene and 0.1 mL of 6 M aqueous acetic acid was added into a 10 mL Schlenk storage tube (SynthwareTM, OD28 x L80mm, high vaccum valve size 0-8mm, with PTFE o-ring, wiper).[26] This mixture was sonicated for 15 mins. in order to get a homogenous dispersion. The tube was then flash frozen at 77 K (liquid N_2 bath) and degassed with three freeze-pump-thaw cycles, and then the tube was sealed and heated at 120 °C for 7 days. A dark red colored precipitate produced was collected by decantation and washed and solvent exchanged with anhydrous tetrahydrofuran (10 mL) several times. The resultants were dried at 120 °C under vacuum overnight to give a light yellow colored powder in 81% (30 mg) isolated yield. FT-IR (KBr, cm^{-1}): 2955 (w), 2925 (w), 2863 (w), 1631 (s, C=O), 1582 (s, C=N), 1501 (s, C=C in enamine), 1451 (s, aromatic C=C), 1141 (s), 829 (s). Anal. Calcld. For $C_{99}O_3H_{63}N_9$: C, 83.35; H, 4.45; N, 8.84%; found: C, 80.55; H, 5.05; N, 8.04%.

Selective dye separation experiment. All the batch adsorption experiments were conducted at r.t. in a dark condition. Initial dye concentrations were fixed to be 50 μM. Typically 5 mg of **SA-COF** was added into 5 mL of dye solution, and the mixture was sonicated by 10 second to get a well-dispersed solution and then stirred at r.t. on hot plate with 700 r.p.m. stirring rate. At appropriate time interval, the mixture was filtered in syringes equipped with Whatman 0.45 μm membrane filters. The concentration of dye in the filtrate was detected using an ultraviolet-visible spectrometer (Shimadzu UV-2600) at a wavelength of maximum absorbance (665, 608 and 664 nm for MB in neutral, basic and acidic condition, respectively; 413 nm for AA in basic condition; 419 nm for CA; 550 nm for RB; 590 nm for DAQ and 546 nm for DHQ). The removal efficiency of dye was calculated as following equation (1):

$$\text{Removal efficiency (\%)} = (C_0 - C_t) / C_0 \times 100 \qquad (1)$$

Where C_0 and C_t are the concentration of dyes at initial condition and in the filtrate, respectively.

For the molecular separation study, 5 mg of **SA-COF** was suspended in 5 mL water solution (pH =12) for 5 mins, and then passed through a Whatman (0.45 μm) membrane filter to give **SA-COF** equipped filter. The resulting **SA-COF** equipped filter was washed with 5 mL water solution (pH =12) once before using it for the separation experiments without any further process.

HPLC was performed with an Agilent 1200 HPLC equipped with a Diode-Array Detector ultraviolet detector and a Phenomenex® Luna C18 (2) column (2.0 x 150 mm, 5 μm particle size). The sample injection volume was 20 μL, and the flow rate was 0.7 mL min^{-1}. The mobile phase for HPLC analysis is 100% methanol. The intensity of the effluent ultraviolet absorbance was monitored at 590 and 468 nm for DAQ and DHQ, respectively. LC calibration curve was created for quantitative analysis using four standard solutions, that is, 1, 10, 50, and 100 μM (Supplementary Fig. S17).

Results and Discussion

Preparation of salicylideneanilines-based covalent organic frameworks. When triformylphloroglucinol ligand with three –OH group is used for synthesis of COFs, it produces a mechanically rigid β-ketoenamine-linked COFs and no reversible proton tautomerism is observed. This is because the strong intramolecular hydrogen bonding interactions pre-

vents the reversible proton tautomerism and locks the COFs in the ketoenamine stage.[27] To circumvent this, we proposed that the incorporation of the 2,4,6-triformayl phenol (**TFP**) moiety with only one –OH group would provide a less rigid β-ketoenamine intermediate and imparts structural flexibility around the pores of the COF needed for undergoing reversible tautomerism.

Phenol, a low-cost and commercially available chemical, was used to synthesize the **TFP** building block in gram scale with 56% yield via a Duff reaction.[28] **SA-COF** was prepared by the solvothermolysis of a suspension of **TFP** and **TAB** (1,3,5-Tris(4-aminophenyl)benzene) in a 5:5:1 (v/v) mixture of 1-buthanol, dichlorobenzene and 6 M aqueous acetic acid (Fig. 1). The Fourier transform infrared (FT-IR) spectra of the **SA-COF** confirm the formation of imine linkage in the polymers, supporting by disappearance of the N−H stretches signals located at 3450 to 3204 cm^{-1} and exhibition of the C=N stretches bands located at 1582 cm^{-1} (Fig. 3a and S2). The characteristic resonance peaks of imine carbons at 158.9 and 156.1 ppm were observed in solid-state 13C cross-polarization/magic angle spinning nuclear magnetic resonance (CP/MAS NMR) spectra of **SA-COF**, evidencing the existence of imine linkages (Fig. 3e). Thermal gravimetric analyses (TGA) under N_2 atmosphere show that **SA-COF** is highly stable up to 500 ^{o}C with only 3.8% weight loss (Fig. S3). Furthermore, scanning electron microscopy (SEM) and (TEM) reveal that it displays plait-like morphology, and consists of highly crystalline nano-flakes (Fig. 2i, j, S5 and S6).

To analyze the crystal structure of obtained polymer **SA-COF**, theoretical simulations and powder X-ray diffraction (PXRD) experiments were performed. The calculations were conducted using Material Studio version 2016 and the eclipsed stacking (AA) and staggered stacking (AB) structures were modeled (See Supporting Information for details). In the experimental PXRD pattern of **SA-COF** (Figure 2a black curve), an intense peak at 5.68° accompanied by four small peaks at 9.76°, 11.20°, 14.89° and ca. 25.16° were observed, which can be assigned to (100), (110), (200), (120) and (001) diffractions. The obtained PXRD pattern matches well with the calculated PXRD pattern of AA stacking structure (Fig. 2a, c), suggesting that **SA-COF** features a highly uniform pore structure with AA stacking model. Specifically, Pawley refinement produces a hexagonal space group with unit cell parameters of $a = b = 18.09$ Å, c= 3.61 Å, α = β = 90°, and γ = 120°, with refinement results of $R_p = 2.91\%$ and $R_{wp} = 4.41\%$. The refined PXRD pattern agrees well with the experimental PXRD data, as confirmed by the vanishing intensity of the difference plot in Fig. 2a,b.

The eclipsed AA stacking structure of **SA-COF** is further supported by the pore size distribution analysis. Nitrogen adsorption−desorption experiment at 77 K (Fig. 2g) exhibits a type I N_2 adsorption isotherm that is characteristic of a microporous structure. The Brunauer−Emmett−Teller (BET) surface area of **SA-COF** is calculated as 1588.56 $m^2 g^{-1}$, and the total pore volume is 0.92 $cm^3 g^{-1}$ ($P/P_0 = 0.99$). The simulated eclipsed-stacked **SA-COF** structure using nonlocal density functional theory (NLDFT) presents a narrow pore size distribution with an average pore width of ~1.43 nm (Fig. 2h), which is very close to the theoretical value of 1.45 nm based on the eclipsed AA stacking structure (Fig. 2e).

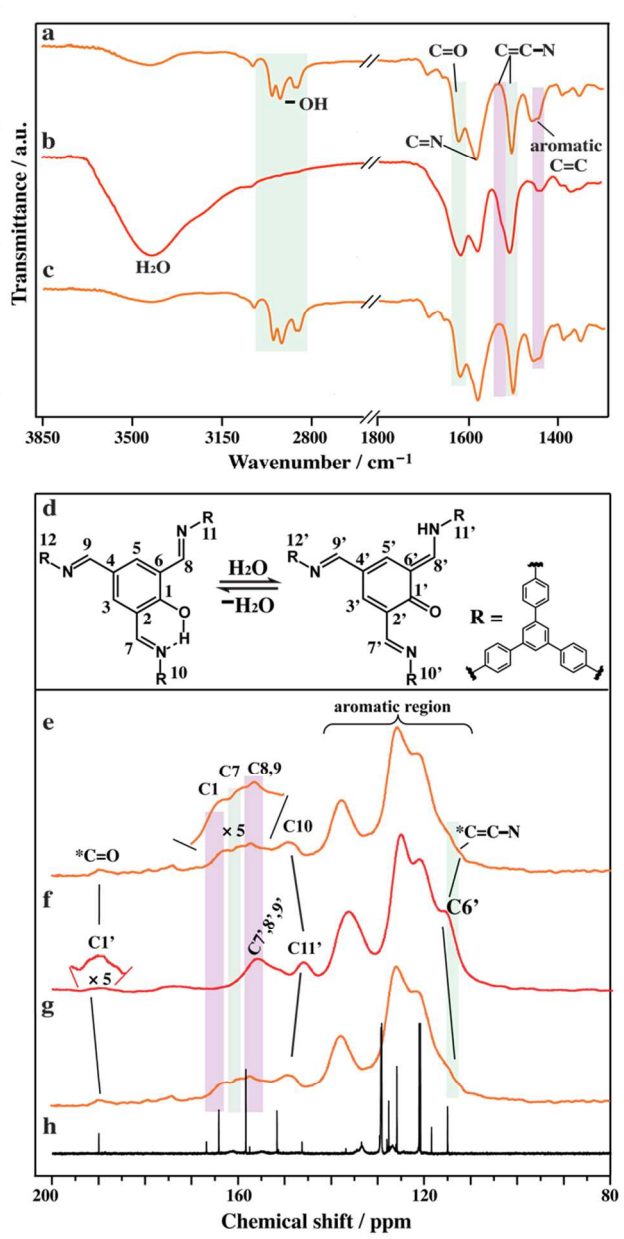

Figure 3. Reversible Proton tautomerism evidenced by FT-IR and solid-state CP/MAS NMR. FT-IR spectra of **a**, dry **SA-COF b**, **SA-COF-H_2O** after exposure to air, and **c**, **SA-COF** after desorption of water from **SA-COF-H_2O**. **d,** schematic presentation of enol and *trans*-keto isomer (the *cis*-keto form is omitted for clarity) Solid-state CP/MAS NMR spectra (100 MHz, 300 K) and assignment of **e**, **SA-COF**; **f**, **SA-COF-H_2O** and **g**, **SA-COF** produced by desorption of water from **SA-COF-H_2O; h,** ^{13}C NMR (500 MHz, 300 K, $CDCl_3$) spectrum of reference compound SA-TFP, exhibiting the co-existence of enol and *cis*-keto form. (*C=O and *C=C-N represent the carbonyl and enamine carbons in *cis*-keto form, respectively)

Proton tautomerism triggered by adsorption and desorption of water. When as-synthesized **SA-COF** powder is exposed to air, its color changes quickly from yellow to deep red (Fig. S2), which hints at the existence of proton tautomerism. To investigate the transformation between enol, *cis*-keto and *trans*-keto form, UV-vis spectroscopic analysis, FT-IR measurement and solid-state CP/MAS NMR studies

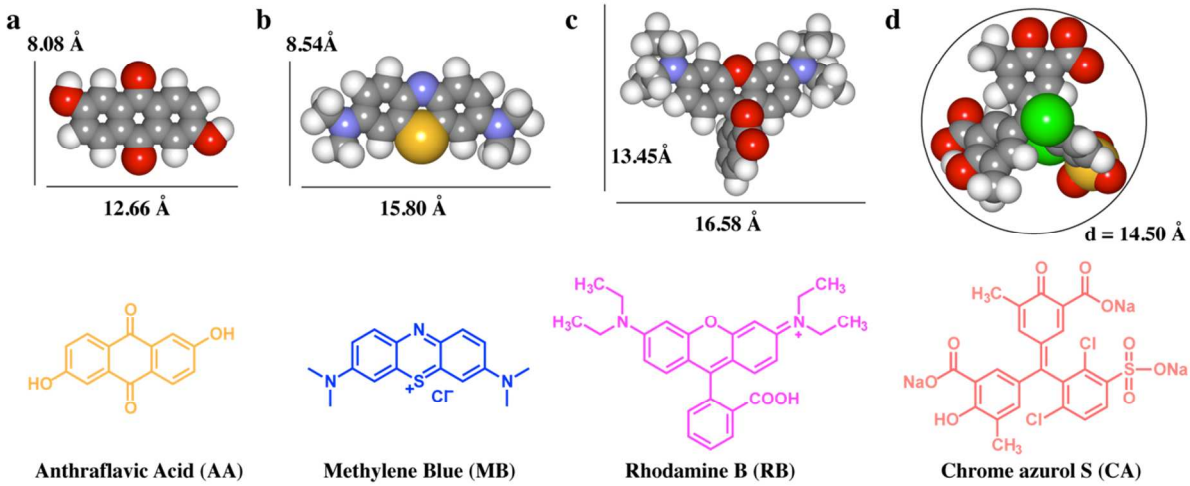

Figure 4. Dye molecules used in molecular separation experiments based on size and charge. Molecular model (top) calculated from Material Studio 2016, displayed in space filling style (Gray, carbon; Red, oxygen; White, hydrogen; Blue, nitrogen; Green, chlorine; Yellow, sulfur.) and chemical structure of dye molecules (bottom); **a**, Anthraflavic acid (AA) with size of 8.08 × 12.66 Å. **b**, Methylene blue (MB) with size of 8.54 × 15.80 Å. **c**, Rhodamine B (RB) with size of 13.45 × 16.58 Å. **d**, Chrome azurol S (CA) with diameter of 14.50 Å.

were conducted. In addition, to better understand the proton tautomerizaion at a molecular level, the molecular reference compound **SA-TFP** was prepared (Fig. 1b), for which the co-exsitence of enol and *cis*-keto form in solution and solid-sate was confirmed by FT-IR, X-ray, Uv-vis and NMR analysis (Fig. 1b and See Supporting Information for details). UV-vis spectroscopy is a sensitive tool for probing the tautomeric equilibrium in **SA** compounds. The band below 425 nm can be attributed to the enol form whereas a contribution peak of *cis*-keto form appears between 425 and 550 nm, and the signals above 550 nm can be assigned to *trans*-keto form.[29,30] The UV-vis spectra of well-dispersed **SA-COF** in anhydrate THF was recorded and it display two major broadened signals at 300 and 450 nm (Fig. S7a), which indicates the co-existence of enol and *cis*-keto form in the pristine **SA-COF** at room temperature. In addition, this result is further supported by UV-vis spectra of the reference compound **SA-TFP**, which shows similar absorption spectrum (Fig. S7b). Without exposure to water molecules, the yellow color of **SA-COF** originates from the *cis*-keto form. To further elucidate the structure of **SA-COF**, FT-IR measurements were conducted. As shown in Fig. 3a, the FT-IR spectra of pristine sample shows a broad absorption band in the region from 3030 to 2850 cm^{-1} similar to that in **SA-TFP** (Fig. S2), which indicates the presence of strong resonance-assisted intermolecular hydrogen bonding, reflected by a large amplitude of O−H stretching vibration or proton transfer equilibrium between O−H enol form and N−H *cis*-keto form.[31] In addition, the intense peaks at 1622 and 1503 cm^{-1} originate from C=O and C=C stretching, confirming the existence of *cis*-keto form. Furthermore, solid-state CP/MAS NMR spectra of **SA-COF** evidence the proton tautomerism between enol and *cis*-keto form and agree well with the UV-vis and FT-IR results. Fig. 3e shows two very weak characteristic ^{13}C resonances of carbonyl (*C=O) and enamine (*C=C−N) carbons at 188.7 and 114.3 ppm, respectively, which are similar to that in the reference compound (190.0 and 115.1 ppm, see Fig. S8), confirming the existence of *cis*-keto form as minor component. Besides, several characteristic ^{13}C resonances of enol form including phenol (C1) and imine (C7, C8 and C9) carbons at 162.2, 158.1 and 156.1 ppm are observed, which are further supported by comparison with ^{13}C NMR spectrum of the reference compound **SA-TFP** (164.3 and 158.4 ppm) (Fig. 3 and S8).[32,33]

When **SA-COF** is exposed to air, it quick absorbs water to give red colored **SA-COF-H_2O**. The UV-vis spectra of well-dispersed **SA-COF-H_2O** in H_2O display two major broad signals at 430 and 587 nm (Fig. S7), indicating the absence of the enol form and the co-existence of *cis*-keto and *trans*-keto form in the **SA-COF-H_2O**. The resulting dark red color of **SA-COF-H_2O** comes from the *trans*-keto form. In addition, the FT-IR profile of **SA-COF-H_2O** (Fig. 3b) further proves the transformation from enol to keto form by the following changes: i) the appearance of a large broad stretching peaks at ~3420 cm^{-1} assignable to absorbed H_2O molecules; ii) the vanishing of the O−H stretching signals located around 2900 cm^{-1}; iii) the increment of peak intensity at 1621 cm^{-1} attributed to C=O stretching; iv) the decrease of signal intensity at 1582 cm^{-1} assigned to C=N stretching; v) appearance of a new peak at 1531 cm^{-1} corresponded to C=C stretching in *trans*-β-ketoenamine, and (vi) the decline of peck intensity at 1450 cm^{-1} assignable to the aromatic C=C stretching. More importantly, the solid-state CP/MAS NMR spectra of **SA-COF-H_2O** (Fig. 3f) also support such transformation by the following evidences: i) increment of signal intensity of carbonyl carbon (C1') at 190.7 ppm corresponding to the increment of *trans*-keto population; ii) low field shift of the *cis*-keto at 188.7 ppm to 190.7 ppm attributed to breaking of intramolecular hydrogen bonding; ii) the disappearance of C1 and C7 resonances in enol form; iii) the rise of peak intensity at 116.3 ppm attributed to C6' resonances in *trans*-keto form. Interestingly, when **SA-COF-H_2O** is heated at 120 ^oC under vacuum, adsorbed water molecules are removed and it returns back to original yellow colored **SA-COF** with identical UV-vis, FT-IR and solid-state CP/MAS NMR spectra (Fig. 3c,g). All these data clearly demonstrate reversible proton tautomerism between enol, *cis*- and *trans*-keto in **SA-COF**, which is readily triggered by the adsorption and desorption of water molecules (See the

proposed mechanism of proton tautomersim in the Supporting Information)

Size-dependent separation. The removal of water-soluble organic pollutants by porous material is an important research field due to rising environmental problems.[34-36] The tunable functionality of pore surface in **SA-COF** induced by proton tautomerism can be exploited for the separation of molecules based on size, charge and functionality. To demonstrate size selective adsorption, we have chosen several water-soluble dye molecules (Fig. 4), specifically Methylene blue (MB), Rhodamine B (RB) and Chrome azurol S (CA). As shown in Fig. 4, the van der Waals sizes of these molecules are calculated using Material Studio 2016. The size of these dye molecules follow the order MB < RB ≲ pore size of **SA-COF** < CA. Ultraviolet-visible (Uv-vis) spectroscopy was used to monitor the change of concentration of dye in fixed time interval. **SA-COF** has the ability to quickly adsorb and remove organic dye (MB) from water (Fig. 5a). The size exclusion effect of **SA-COF** was tested by selecting three molecules with different sizes, and we found that the binding affinity of **SA-COF** for dye molecules declines with an increase in molecular size. As shown in Fig. 5b, the smallest size MB was completely removed within 10 minutes, showing a removal efficiency of 98.3%, while the larger size RB, which is slightly smaller than the pore size of **SA-COF**, exhibits a much slower adsorption rate (~ 60 mins), and with 94.1% removal efficiency compared to that of MB. The largest dye, CA, whose size is larger than 1.45 nm, exhibits no noticeable change of its concentration during the adsorption tests (Fig. 5b). Meanwhile, when the dye MB and CA were treated with commercial porous activated carbon, it does not show good separation performance (See Fig. S16). The size-dependent adsorption reflects the highly uniform pore size distribution of **SA-COF** (~1.43 nm), rendering it a useful molecular sieve material based on size-exclusion. To test this, **SA-COF** powders was suspended and stirred in a green colored aqueous solution of MB and CA (1:1 molar ratio) for 10 mins. at r.t. After filtration, the UV-vis spectra before and after **SA-COF** treatment show that the MB and CA mixture can be completely separated, the concentration of MB is decreased by 99.9%, while CA does not show any notable change (Fig. 5d). It should be stated here that the size of the dye molecule may not be the only factor at play, charge and functional groups in the dye molecules may act in concert with its size to effect size-dependent adsorption in the **SA-COF**.

Charge selective separation. Since the –OH or –NH moieties in **SA-COF** can be deprotonated or protonated in basic or acidic condition, respectively, **SA-COF** is expected to a promising platform for separation of charged molecules due to its pH-controllable ionicity. Before the separation test, the stability of **SA-COF** in base (pH = 12, 0.01 M NaOH) or acid (pH = 1, 0.1 M HCl) was examined. **SA-COF** retained its original crystalline structure in base or acid, as indicated by the unchanged intensities and positions of the peaks in its PXRD profile (Fig. S12). **SA-COF** powder was added to an aqueous solution of Anthraflavic acid (AA) (Fig. 4a), a negative charged dye at basic condition (pH = 12), and no remarkable change in the concentration of AA was found, as confirmed by UV-vis spectroscopy (Fig. 5b, S11). In contrast, MB, which has a similar size to AA but positive charged instead, was rapidly absorbed within 10 seconds (99.8% removal efficiency) at the same condition (Fig. 5b), showing a large increment of uptake rate compared to the neutral **SA-COF** (98.3% removal efficiency at 10 mins.), suggesting that electrostatic attraction is operational here. However, when the dye AA and MB were treated with

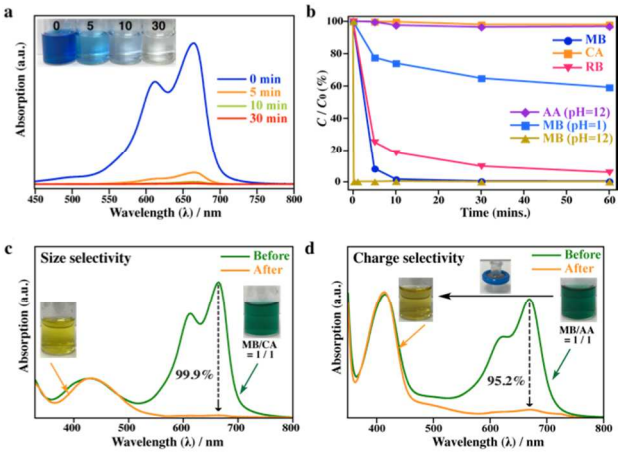

Figure 5. Size and charge-selective separation experiments. **a,** UV-vis absorption spectra of an aqueous solution of MB after treatment with **SA-COF** at different intervals. **b**, Change in concentration of dye over time after treatment with **SA-COF,** determined by change in absorbance relative to initial absorbance (C / C_0). The data is averaged over three test trials. **c**, UV–vis absorption spectra of size-selective separation of CA from a mixture of CA and MB in water (green and orange line represent before and after treatment with **SA-COF**, respectively; inset, photographs of CA and MB mixture and filtrate after treatment with **SA-COF**, showing green and deep yellow color). **d**, UV–vis absorption spectra of charge- selective separation of AA from mixture of AA and MB in water (green and orange line represent before and after treatment with **SA-COF**, respectively; inset, photo-image of green colored CA and MB mixture, deep yellow colored filtrate after passing though the filter disc charged with **SA-COF** powders)

commercial porous activated carbon at the same condition, it does not show any selective separation (See Fig. S16). To further test the charge separation effect, a green colored AA and MB mixture in 1:1 ratio was quickly passed through (~ 10 seconds) a filter in which the base treated **SA-COF** powders were pre-equipped (details see experimental section). The UV-vis spectra before and after filter treatment revealed that the AA and MB mixture was clearly separated, and there was a sharp decrease of MB concentration (95.2%) (Fig. 5d), however, almost no change was observed for concentration of AA. More interestingly, the absorption ability of **SA-COF** toward MB can be reversed. When the **SA-COF** powder was added into an acidic aqueous solution of MB, the concentration of MB showed a much slower decrease with 22% removal efficiency within 5 mins (Fig. 5b) than that in basic condition (99.8% removal efficiency at 10 seconds).

Chemo-selective separation. Owing to the basic N–H moiety in the *trans*-keto form, **SA-COF** can discriminate functional groups with different acidity and it selectively bind –OH over $–NH_2$ groups under neutral condition. Two molecules of the same size, but with different functional groups, 1,4-dihydroxyanthraquinone (DHQ) and 1,4-diaminoanthraquinone (DAQ), are chosen as model compound (Fig. 6a). **SA-COF** powder was added to a solution of DHQ in ethanol and water mixed solvent (V_{EtOH}/V_{H2O} = 2/3),

and a significant decrease in concentration of DHQ with almost 90% removal efficiency within 60 mins was observed by UV-vis spectroscopy. In contrast, the concentration of DAQ was slightly only decreased with ~ 25% removal efficiency within 60 mins, resulting a high selectivity with a

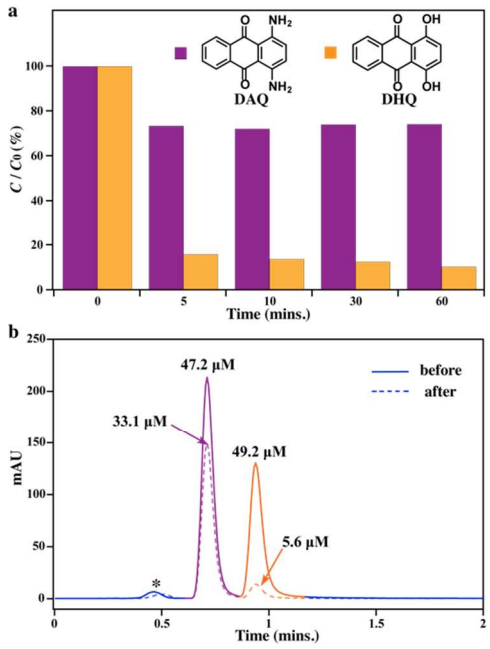

Figure 6. Chemo-selective separation experiments. **a,** UV visible absorbance spectra of DAQ and DHQ at different time interval after treatment with **SA-COF** (purple, DAQ; orange, DHQ) The data are average of triplicate experiments. **b,** HPLC spectra of DAQ and DHQ mixture in 1:1 molar ratio before and after treatment with **SA-COF** (full line: before; dotted line: after; purple (DAQ) and orange (DHQ) peaks with 0.693 and 0.914 mins retention times, respectively. The * marked peak represent the solvent peak)

ratio of 1:7 for DHQ : DAQ in the filtrate (Fig. 6a). The molecular selectivity is further demonstrated in a separation experiment: when a 1:1 mixture of DHQ and DAQ was treated with **SA-COF** powder, within 10 mins, the ratio for DHQ:DAQ were found to be 1:6 in the filtrate, as confirmed by the HPLC analysis (Fig. 6b).

Conclusion

We have successfully synthesized salicylideneanilines-based COF, which exhibits reversible solvatochromism triggered by adsorption and desorption of water molecules. Our studies show that inborn, chemo-responsive pores can be programmed into COF by reticular synthesis. The reversible proton tautomerism was confirmed by UV-vis spectroscopy, FT-IR and solid-state CP/MAS NMR analysis. The tautomerization of **SA-COF** stimulates dynamic changes in the ionic and chemical properties of the pores and allows molecular separation on the basis of size-exclusion, charge separation and functional group discrimination. Specifically, it binds positively charged molecules in basic condition, while excluding them in acidic condition. Moreover, **SA-COF** can discriminate functional groups with different degree of acidity i.e. it prefers to bind to molecules with aromatic hydroxyl groups rather than aromatic amino groups. Our studies open an avenue for designing smart, chemo-responsive COFs, further attesting to the utility of COFs as flexible and tunable materials for molecular separation application.

ASSOCIATED CONTENT

Supporting Information

The Supporting Information is available free of charge on the ACS Publications website.

Additional experimental procedures and structural modeling, IR, TGA, BET analysis, SEM and TEM images, Uv-vis spectrum, Solid-state CP/MAS NMR spectra, the proposed mechanism of proton tautomersim, selectivity experiment, control experiment and HPLC analysis (PDF)

AUTHOR INFORMATION

Corresponding Author

* chmlohkp@nus.edu.sg

Notes

The authors declare no competing financial interests.

ACKNOWLEDGMENT

K. P. Loh acknowledges NRF-CRP grant "Two Dimensional Covalent Organic Framework: Synthesis and Applications." Grant number NRF-CRP16-2015-02, funded by National Research Foundation, Prime Minister's Office, Singapore.

REFERENCES

(1) Adrien P. Côté, A. P., Benin, A. I., Ockwig, N. W., O'Keeffe, M., Matzger, A. J., Yaghi, O. M. *Science* **2005**, *310*, 1166–1170.
(2) Waller, P. J., Gándara, F., Yaghi, O. M. *Acc. Chem. Res.* **2015**, *48*, 3053–3063.
(3) Feng, X., Ding, X., Jiang, D. *Chem. Soc. Res.* **2012**, *41*, 6010–6022.
(4) Ding, S. Y., Wang, W. *Chem. Soc. Rev.* **2013**, *42*, 548–568.
(5) Slater, A. G., Cooper, A. I. *Science* **2015**, *348*, aaa8075.
(6) Doonan, C. J., Tranchemontagne, D. J., Glover, T. G., Hunt, J. R., Yaghi O. M. *Nat. Chem.* 2010, *2*, 235–238.
(7) Huang, N., Krishna, R., Jiang, D. *J. Am. Chem. Soc.* **2015**, *37*, 7079–7082.
(8) DeBlase, C. R., Silberstein, K. E., Truong, T.-T., Abruña, H. D., Dichtel, W. R. *J. Am. Chem. Soc.* **2015**, *135*, 16821–16824.
(9) Xu, F., Jin, S., Zhong, H., Wu, D., Yang, X., Chen, X., Wei, H., Fu. R., Jiang, D. *Sci. Rep.* **2015**, 5, 8225.
(10) Liu, W., Luo, X., Bao, Y., Liu, Y. P., Ning, G.-H., Abdelwahab, I., Li, L., Nai, C. T., Hu, Z. G., Zhao, D., Liu, B., Quek, S.Y., Loh, K. P. *Nat. Chem.* **2017**, *9*, 563-570.
(11) (a) Fang, Q., Wang, J., Gu, S., Kaspar, R. B., Zhuang, Z., Zheng, J., Guo, H., Qiu, S., Yan, Y. *J. Am. Chem. Soc.*, **2015**, *137*, 8352–8355; (b) Fang, Q., Zhuang, Z., Gu, S., Kaspar, R. B., Zheng, J., Wang, J., Qiu, S., Yan, Y. *Nat. Commun.* **2014**, *5*, 4503.
(12) Ding, S.-Y., Gao, J., Wang, Q., Zhang, Y., Song, W.-G., Su, C.-Y., Wang, W. *J. Am. Chem. Soc.*, **2011**, *133*, 19816–19822.
(13) Lin, S., Diercks, C. S., Zhang, Y.-B., Kornienko, N., Nichols, E. M., Zhao, Y., Paris, A. R., Kim, D., Yang, P., Yaghi, O. M., Chang, C. J. *Science* **2015**, *349*, 1208–1213.
(14) Xu, H., Gao, J., Jiang, D. *Nat. Chem.* **2015**, *7*, 905–912.

(15) Ding, X., Guo, J., Feng, X., Honsho, Y., Guo, J., Seki, S., Maitarad, P., Saeki, A., Nagase, S., Jiang, D. *Angew. Chem. Int. Ed.* **2011**, *50*, 1289–1293.
(16) Guo, J., Xu, Y., Jin, S., Chen, L., Kaji, T., Honsho, Y., Addicoat, M. A., Kim, J., Saeki, A., Ihee, H., Seki, S., Irle, S., Hiramoto, M., Gao, J., Jiang, D. *Nat. Commun.* **2013**, 4, 2736.
(17) Xu, H., Tao, S., Jiang, D. *Nat. Mater.* **2016**, *15*, 722–726.
(18) Ding, S.-Y., Dong, M., Wang, Y.-W., Chen, Y.-T., Wang, H.-Z., Su, C.-Y., Wang, W. *J. Am. Chem. Soc.*, **2016**, *138*, 3031–3037.
(19) Cohen, M. D., Schmidt, G. M. J., Flavian, S. *J. Chem. Soc.*, **1964**, 2041–2051.
(20) Hadjoudis, E., Vittorakis, M., Mavridis, I. M. *Tetrahedron* **1987**, *43*, 1345–1360.
(21) Amimoto, K., Kawato, T. *J. Photochem. Photobiol., C,* **2005**, *6*, 207–226.
(22) Hadjoudis, E., Mavridis, I. M. *Chem. Soc. Res.* **2004**, *33*, 579–588.
(23) Cohen, M. D., Flavian, S., Leiserowitz, L. *J. Chem. Soc.*, *B,* **1967**, 329–334.
(24) Ogawa, K., Kasahara, Y., Ohtani, Y., Harada, J. *J. Am. Chem. Soc.*, **1998**, *120*, 7107–7108.
(25) Harada, J., Uekusa, H., Ohashi, Y. *J. Am. Chem. Soc.*, **1999**, *121*, 5809–5810.
(26) (a) Gao, Q., Bai, L., Zeng, Y., Wang, P., Zhang, X., Zou, R., Zhao, Y. *Chem. Eur. J.* **2015**, *21*, 16818–16822; (b) Gao, Q., Bai, L., Zhang, X., Wang, P., Li, P., Zeng, Y., Zou, R., Zhao, Y. *Chin. J. Chem.* **2015**, *33*, 90-94.
(27) Kandambeth, S., Mallick, A., Lukose, B., Mane, M. V., Heine, T., Banerjee, R. *J. Am. Chem. Soc.*, **2012**, *134*, 19524–19527.
(28) Anderson, A. A., Goetzen, T., Shackelford, S. A., Tsank, S. *Synth. Commun.*, **2007**, *30*, 3227–3232.
(29) Fujiwara, T., Harada, J., Ogawa, K., *J. Phys. Chem. B*, **2004**, *108*, 4035–4038.
(30) Jacquemin, P.-L., Robeyns, K., Devillers, M., Garcia, Y. *Chem. Eur. J.* **2015**, *21*, 6832–6845.
(31) Ambroziaka, K., Rozwadowskia, Z., Dziembowskaa, T., Biegb, B. *J. Mol. Struct.* **2002**, *615*, 109–120.
(32) Schilfa, W., Kamieńskia, B., Kołodziejb, B., Grechb, E., Rozwadowskib, Z., Dziembowskab, T. *J. Mol. Struct.* **2002**, *615*, 141–146.
(33) Claramunt, R. M., López, C., María, M. D. S., Sanz, D. and Elguero, J. *Prog. NMR Spectrosc*. **2006**, *49*, 169–206.
(34) Schwarzenbach, R. P., Escher, B. I., Fenner, K., Hofstetter, T. B., Johnson, C. A., Gunten, U., Wehrli, B. *Science* **2006**, *313*, 1072–1077.
(35) Alsbaiee1, A., Smith, B. J., Xiao, L., Ling, Y., Helbling, D. E., Dichtel, W. R. *Nature* **2016**, *529*, 190–194.
(36) Byun, J., Patel, H. A., Thirion, D., Yavuz, C. T. *Nat. Commun.* **2016**, *7*, 13377.

TOC

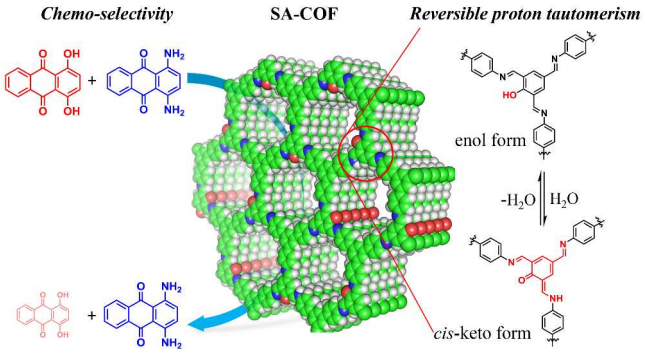
Chemo-selectivity
SA-COF
Reversible proton tautomerism
enol form
-H2O
H2O
cis-keto form